Alfvén Waves in the Solar Corona
S. Tomczyk, *et al.*
Science **317**, 1192 (2007);
DOI: 10.1126/science.1143304

conformation and reactivity of the epoxy alcohols (**5**, **15**, and **17**). Nevertheless, as shown in Fig. 4 (**20**), activation of the nucleophile (OH group) and electrophile (epoxide) may be achieved by two water molecules (red and blue H_2O, respectively) in a cooperative network of hydrogen bonds that would account for not only the enhanced regioselectivity in water (relative to other solvents), but also the marginal effects of temperature on selectivity. Another possibility (**21**) is analogous to the dual-H-bond mode of activation (red H_2O) in epoxide hydrolases, but because activation of the electrophile is disconnected from that of the nucleophile, this model less easily explains the selectivity.

More complex hybrids that unite the attributes of these two models can also be posited, but at this stage we favor **20** for several reasons. Its relative simplicity (i.e., lower molecularity) constitutes a more easily testable structural hypothesis, and the results observed with methanol and ethylene glycol are also adequately explained, in the forms of **22** and **23**, respectively. Furthermore, as illustrated in **23**, ethylene glycol represents an attractive starting point for the development of small molecules that activate the nucleophile and electrophile in such a way as to effect cyclizations and cascades of even higher selectivity and efficiency. In the meantime, templated, water-promoted, THP-selective epoxide-opening cascades provide a straightforward means for efficient and rapid assembly of ladder polyethers, enabling investigations directed toward understanding the mode of action of these extraordinary natural products.

References and Notes

1. Y.-Y. Lin *et al.*, *J. Am. Chem. Soc.* **103**, 6773 (1981).
2. K. C. Nicolaou *et al.*, *J. Am. Chem. Soc.* **117**, 1173 (1995).
3. K. C. Nicolaou *et al.*, *Nature* **392**, 264 (1998).
4. M. Hirama *et al.*, *Science* **294**, 1904 (2001).
5. V. L. Trainer, D. G. Baden, W. A. Catterall, *J. Biol. Chem.* **269**, 19904 (1994).
6. M. S. Lee, D. J. Repeta, K. Nakanishi, M. G. Zagorski, *J. Am. Chem. Soc.* **108**, 7855 (1986).
7. H.-N. Chou, Y. Shimizu, *J. Am. Chem. Soc.* **109**, 2184 (1987).
8. R. V. Snyder *et al.*, *Phytochemistry* **66**, 1767 (2005).
9. K. Nakanishi, *Toxicon* **23**, 473 (1985).
10. J. M. Coxon, M. P. Hartshorn, W. H. Swallow, *Aust. J. Chem.* **26**, 2521 (1973).
11. Baldwin's rules for ring closure classify the fused and spiro transition states as endo and exo processes, respectively. However, because the epoxide C–O bond that breaks is outside the newly formed ring in both cases, each may also be considered to be an exo process under the same construct. [See (*37*).] Thus, to avoid potential confusion, we prefer the distinct terms "fused" and "spiro."
12. The fused/spiro nomenclature is commonly used in cyclopropane-opening reactions (*38*).
13. Many effective directing groups have been developed. For the pioneering work in this area, see (*39*).
14. K. D. Janda, C. G. Shevlin, R. A. Lerner, *Science* **259**, 490 (1993).
15. M. Tokunaga, J. F. Larrow, F. Kakiuchi, E. N. Jacobsen, *Science* **277**, 936 (1997).
16. M. H. Wu, K. B. Hansen, E. N. Jacobsen, *Angew. Chem. Int. Ed.* **38**, 2012 (1999).
17. T. Tokiwano, K. Fujiwara, A. Murai, *Synlett* 335 (2000).
18. F. Bravo, F. E. McDonald, W. A. Neiwert, B. Do, K. I. Hardcastle, *Org. Lett.* **5**, 2123 (2003).
19. G. L. Simpson, T. P. Heffron, E. Merino, T. F. Jamison, *J. Am. Chem. Soc.* **128**, 1056 (2006).
20. T. P. Heffron, T. F. Jamison, *Synlett* 2329 (2006).
21. Materials and methods are available as supporting material on *Science* Online.
22. Y. Tu, Z.-X. Wang, Y. Shi, *J. Am. Chem. Soc.* **118**, 9806 (1996).
23. S. Wan, H. Gunaydin, K. N. Houk, P. E. Floreancig, *J. Am. Chem. Soc.* **129**, 7915 (2007).
24. W. C. Still, A. G. Romero, *J. Am. Chem. Soc.* **108**, 2105 (1986).
25. S. L. Schreiber *et al.*, *J. Am. Chem. Soc.* **108**, 2106 (1986).
26. D. E. Cane, W. B. Celmer, J. W. Westley, *J. Am. Chem. Soc.* **105**, 3594 (1983).
27. C. M. Kleiner, P. R. Schreiner, *Chem. Commun.* 4315 (2006).
28. A. R. Gallimore *et al.*, *Chem. Biol.* **13**, 453 (2006).
29. P. Wernet *et al.*, *Science* **304**, 995 (2004).
30. J. D. Smith *et al.*, *Science* **306**, 851 (2004).
31. E. Vöhringer-Martinez *et al.*, *Science* **315**, 497 (2007).
32. D. C. Rideout, R. Breslow, *J. Am. Chem. Soc.* **102**, 7816 (1980).
33. U. M. Lindstrom, *Chem. Rev.* **102**, 2751 (2002).
34. S. Narayan *et al.*, *Angew. Chem. Int. Ed.* **44**, 3275 (2005).
35. C.-J. Li, L. Chen, *Chem. Soc. Rev.* **35**, 68 (2006).
36. Z. Su, Y. Xu, *Angew. Chem.* **46**, 6163 (2007).
37. J. E. Baldwin, *J. Chem. Soc. Chem. Commun.* **18**, 734 (1976).
38. S. J. Danishefsky, J. Dynak, E. Hatch, M. Yamamoto, *J. Am. Chem. Soc.* **96**, 1256 (1974).
39. K. C. Nicolaou *et al.*, *J. Am. Chem. Soc.* **111**, 5330 (1989).

40. Financial support was provided by the NIH National Institute of General Medical Sciences (grant R01 GM-72566) and by gifts from Merck Research Laboratories and Boehringer Ingelheim. I.V. is grateful to the Massachusetts Institute of Technology for a Nicholas A. Milas Fellowship.

Supporting Online Material

www.sciencemag.org/cgi/content/full/317/5842/1189/DC1
Materials and Methods
Schemes S1 to S5
Table S1
References

13 June 2007; accepted 18 July 2007
10.1126/science.1146421

REPORTS

Alfvén Waves in the Solar Corona

S. Tomczyk,[1]* S. W. McIntosh,[1,2] S. L. Keil,[3] P. G. Judge,[1] T. Schad,[4] D. H. Seeley,[5] J. Edmondson[6]

Alfvén waves, transverse incompressible magnetic oscillations, have been proposed as a possible mechanism to heat the Sun's corona to millions of degrees by transporting convective energy from the photosphere into the diffuse corona. We report the detection of Alfvén waves in intensity, line-of-sight velocity, and linear polarization images of the solar corona taken using the FeXIII 1074.7-nanometer coronal emission line with the Coronal Multi-Channel Polarimeter (CoMP) instrument at the National Solar Observatory, New Mexico. Ubiquitous upward propagating waves were seen, with phase speeds of 1 to 4 megameters per second and trajectories consistent with the direction of the magnetic field inferred from the linear polarization measurements. An estimate of the energy carried by the waves that we spatially resolved indicates that they are too weak to heat the solar corona; however, unresolved Alfvén waves may carry sufficient energy.

Alfvén (*1*) first postulated the existence of oscillations of magnetized plasma in 1942. Of the three possible magnetohydrodynamic (MHD) wave modes, the slow and fast magnetoacoustic (MA) modes are compressible and susceptible to damping. The third so-called Alfvén mode is an incompressible transverse oscillation that propagates along field lines with magnetic tension as the restoring force. Following Alfvén's initial work, researchers soon realized that Alfvén waves could transport energy from the turbulent solar photosphere into the solar corona (*2*, *3*) and might explain one of the most important puzzles in solar physics: Why does the temperature of the solar atmosphere rise from 5000 to 2 million degrees Kelvin from the photosphere outward to the corona?

Over the past decade, the variety of wave phenomena observed in the solar corona has increased enormously. Transverse displacement

[1]High Altitude Observatory (HAO), National Center for Atmospheric Research (NCAR), Post Office Box 3000, Boulder, CO 80307–3000, USA. [2]Department of Space Studies, Southwest Research Institute, 1050 Walnut Street, Suite 300, Boulder, CO 80302, USA. [3]National Solar Observatory, Sacramento Peak Observatory, 1 Loop Drive, Sunspot, NM 88349, USA. [4]Physics Department, University of Notre Dame, 225 Nieuwland Science Hall, Notre Dame, IN 46556–5670, USA. [5]Framingham High School, 115 A Street, Framingham, MA 01701, USA. [6]Department of Atmospheric, Oceanic, and Space Sciences, University of Michigan, 2455 Hayward Street, Ann Arbor, MI 48109–2143, USA.

*To whom correspondence should be addressed. E-mail: tomczyk@ucar.edu

oscillations associated with fast MA kink waves have been observed with the Transition Region and Coronal Explorer satellite (*4*, *5*). Intensity fluctuations associated with propagating slow-mode MA waves have been observed, with periods between 10 and 15 min in polar plumes with the Extreme Ultraviolet Imaging Telescope (EIT) on the Solar and Heliospheric Observatory (SOHO) (*6*) and in coronal loops with periods near 5 min in the extreme ultraviolet (*7*, *8*) and at visible wavelengths (*9*). High-frequency intensity oscillations have been seen during eclipses (*10*, *11*). Also, observations of coronal velocity fluctuations (*12*, *13*) have revealed waves with periods near 5 min.

Alfvén waves have been detected through in situ measurements of the solar wind for several decades (*14*); however, their definitive observation in coronal plasma is lacking for two reasons. First, Alfvén waves are incompressible, so they are not visible as intensity fluctuations; the intensity imagers used for most coronal observations will not see them. Second, velocity fluctuations inferred from Doppler shifts of emission lines require spectrograph or narrow-band filtergraph measurements; most coronal work has been performed with spectrographs that cannot observe over a large enough field of view in a time that is sufficiently short compared to the wave periods.

Here, we present results from the Coronal Multi-Channel Polarimeter (CoMP), a combination tunable filter and polarimeter that can measure properties of infrared coronal emission lines across a large field of view with short integration times [Supporting Online Material (SOM) text]. The CoMP instrument observes the complete polarization state of light through a 0.13-nm filter bandpass that is tuned to three wavelengths across the FeXIII coronal emission line at 1074.7 nm. The measured polarization state is parameterized by a Stokes vector [I, Q, U, V], where I is the intensity, Q and U describe net linear polarization states, and V describes the net circular polarization. Observations consisting of images of the corona between 1.05 and ~1.35 solar radii (R_{sun}) in the four Stokes parameters at the wavelengths 1074.52, 1074.65, and 1074.78 nm were obtained every 29 s on 30 October 2005 between 14.261 and 23.562 hours UT, with a spatial sampling of 4.5 arc sec per pixel.

After detector calibrations (SOM text), we determined the motion of the images during the day with a cross-correlation technique and translated the images to a common center. Lastly, the images were interpolated in time onto a grid with a constant spacing of 29 s. We selected a subarray of the data on the east limb for further analysis. This region included active region loops and a coronal cavity (Fig. 1A).

For each point in the selected subarray and each image in the time series, the central intensity of the line, the central wavelength, and the line width were obtained from a Gaussian fit to the intensity (Stokes I) at the three wavelengths. The line-of-sight (LOS) velocity was determined from the Doppler shift of the central wavelength from the rest wavelength of the emission line. Also, the degree of linear polarization, p, and the direction of the magnetic field (azimuth) in the plane of the sky (POS), ϕ, were obtained from Stokes I, Q, and U using only the central (1074.65-nm) bandpass from the relations

$$p = (Q^2 + U^2)^{1/2}/I \quad (1)$$

$$\phi = \tfrac{1}{2}\tan^{-1}(U/Q) \quad (2)$$

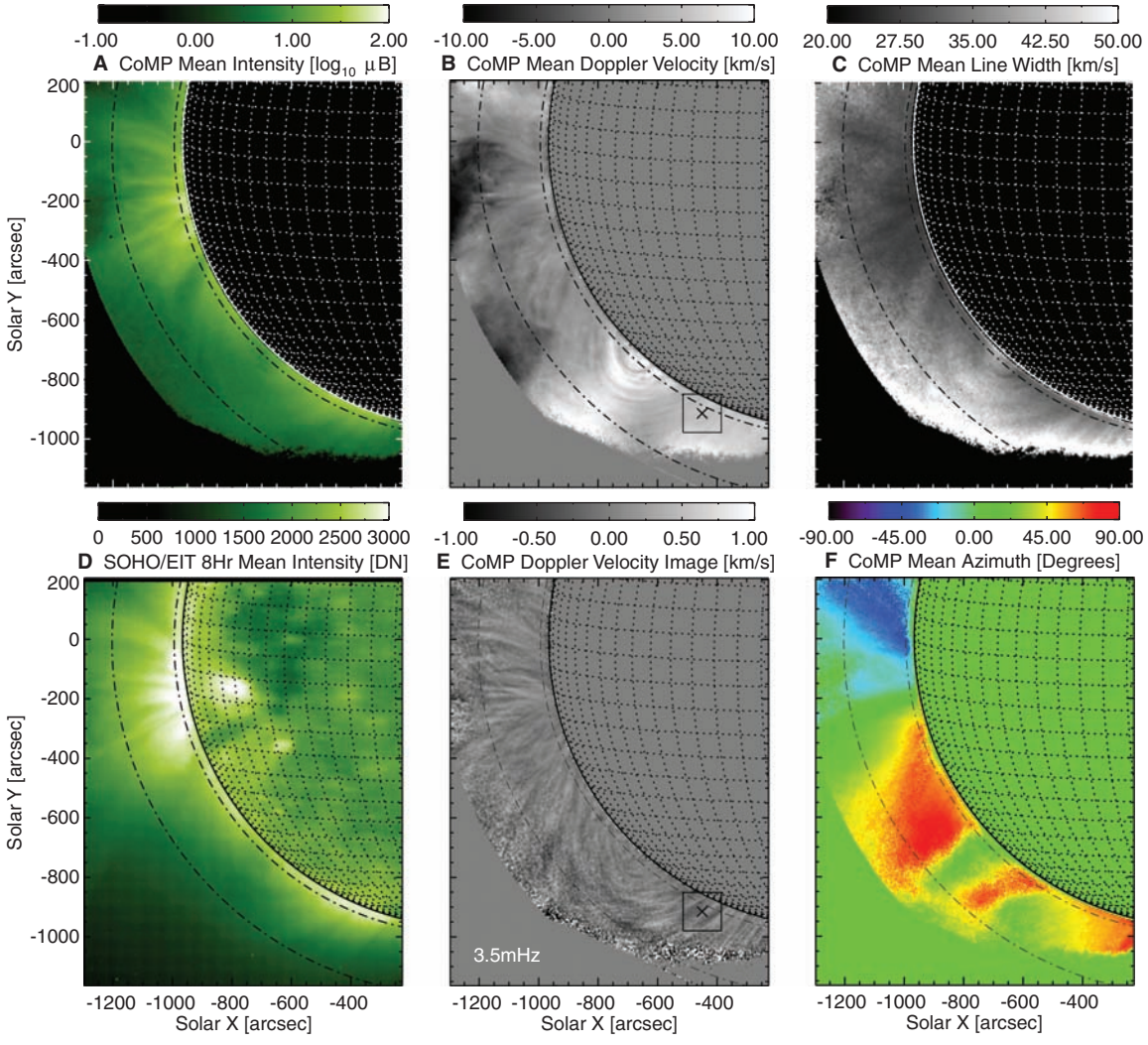

Fig. 1. From left to right, top to bottom, the CoMP observations of time-averaged intensity (**A**), Doppler velocity (**B**), line width (**C**), 3.5-mHz filtered Doppler velocity snapshot (**E**), and POS azimuth (**F**). In addition, we show the SOHO/EIT 19.5-nm image averaged over the same time (**D**). DN, data number (the unit of brightness). (B) and (E) include the location (X) and surrounding square region used in the example of the travel-time analysis. Dot-dashed lines representing distances of 5 and 25% of R_{sun} (above the limb) that are used as limits to our analysis are indicated.

where ϕ has the well-known ambiguity of 90° (*15*), which does not affect the conclusions of the following analysis.

A movie of the velocity images (movies S2 and S4) reveals ubiquitous quasi-periodic fluctuations with root means square amplitude of about 0.3 km s^{-1}. The time series of intensity images does not reveal appreciable variation with fractional fluctuations, $\Delta I/I < 3 \times 10^{-3}$. A Fourier analysis (Fig. 2) of the region of bright active region loops shows a significant, broad peak in the power spectrum of velocity fluctuations centered at ~3.5 mHz (5-min period) with a width of about 1 mHz. Such a peak is absent in the power spectrum of intensity fluctuations or line width. The background spectrum at low frequencies rises as 1/frequency^2 due presumably to instrumental noise and coronal evolution. We find that the observed spectrum of velocity power is remarkably similar to the power spectrum of photospheric 5-min oscillations, and we note that the frequency distribution of velocity power is nearly identical for both the coronal cavity and the active loop regions.

We adapted a phase travel-time analysis (*16*–*18*) to characterize the propagation characteristics of the wave modes observed in the CoMP velocity time series. The data were Fourier filtered in time with a Gaussian filter with a central frequency of 3.5 mHz and a width (1/e folding) of 0.4 mHz. We then formed the cross-correlation map of the filtered time series at a reference pixel with nearby pixels sufficient in number to capture all areas of high correlation. The cross-correlation function with neighboring pixels is a Gabor wavelet that yields information about the group and phase travel times of the fluctuation (*17*). We see (Fig. 3A) that the observed oscillations can have very long correlation lengths (the length of the oblong contour of high cross-correlation) and detectable widths. The "island" of high cross-correlation (CC > 0.5) also has a distinct direction that follows the apparent trajectory of the propagating wave, as seen in movies S2 and S4.

By using the island of high cross-correlation as a mask, we computed the correlation length, the correlation width, the phase speed of the propagation, and the propagation angle relative to solar north-south. We used the cross-correlation weighted least-squares fit to the points inside the island to estimate the propagation angle and its associated error. In addition, by isolating the phase travel times in the island and computing the distance of each pixel to the reference pixel, we estimated the phase speed (and standard error) of the wave from the least-squares fit of the distance and phase travel time. In the example shown in Fig. 3, we computed a correlation length of 45 Mm, a width of 9 Mm, a propagation trajectory of 46.2° (±4.0°), and a phase speed of 1.31 (±0.24) Mm s^{-1} at the reference pixel. Note that the measured phase speeds are POS projections and are therefore lower limits. This travel-time analysis was repeated, successively substituting all pixels between 1.05 and 1.25 R_{sun} (dot-dashed lines in Fig. 1) as the reference pixel, to extract the wave properties at each point (Fig. 4 and table S1).

The CoMP instrument can infer the POS azimuth of the coronal magnetic field through the linear polarization measurements and Eq. 2 (Fig. 1F). This angle is compared with the angle of wave propagation inferred from the travel-time analysis (Fig. 4B) in Fig. 4F. Despite the fact that LOS integrations may influence the two angles differently, the high degree of correlation in this plot demonstrates that the waves propagate along field lines.

We believe that the waves we observe are Alfvén waves, for the following three reasons. The observed phase speeds (~2 Mm s^{-1}) are much larger than the sound speed (~0.2 Mm s^{-1}), and therefore the waves are not slow MA mode waves. The spatiotemporal properties of the velocity oscillations and the linear polarization measurements show that these waves propagate along field lines, which would not be the case for fast MA mode waves. In addition, the associated intensity fluctuations are very small. A source of waves distributed across the solar surface would not produce the coherent spatial structures aligned with the magnetic field, which are present in the velocity data.

The presence of a 5-min signature is not surprising because fluctuations in the corona with periods near 5 min have been widely observed, as discussed above. There is a growing consensus that photospheric 5-min acoustic oscillation modes (p modes) escape into higher layers via interactions with surface magnetic fields. In the

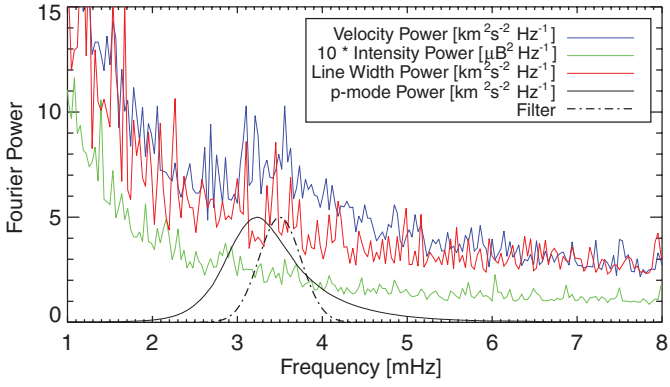

Fig. 2. Fourier power spectrum of the CoMP Doppler velocity (blue), intensity (green), and line width (red). Notice the significant, broad peak in the Doppler power spectrum centered on 3.5 mHz. We also show the (scaled) Gaussian filter applied in the analysis (dot-dashed black line) and the average power spectrum of intermediate degree photospheric oscillations (solid black line).

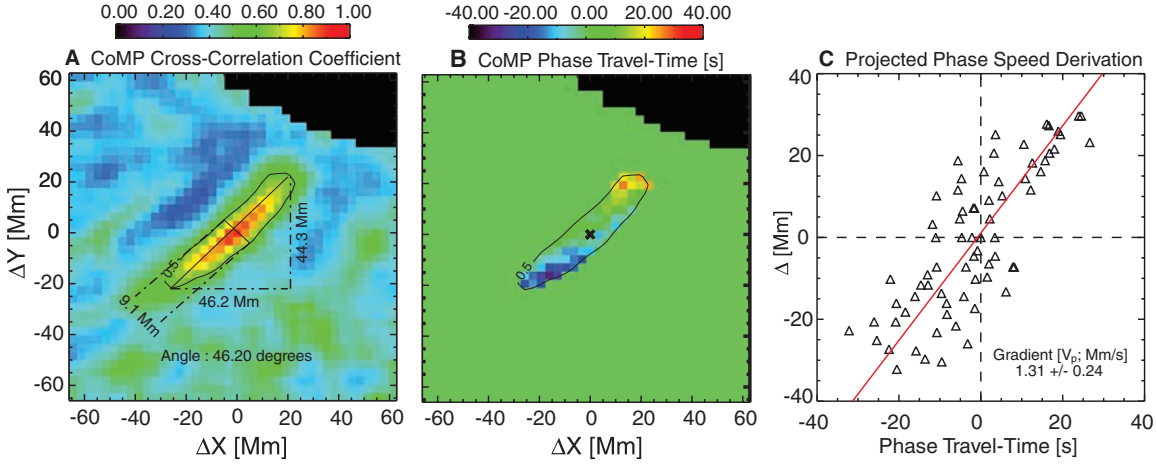

Fig. 3. Travel-time analysis of CoMP Doppler velocity measurements for the reference pixel (marked by the x) over the boxed region shown in Fig. 1. (**A**) The map of cross-correlation coefficients with a contour of 0.5, which is used to define the region used to determine the properties of the waves. (**B**) The map of computed phase travel times in the same region (the surrounding pixels are zeroed for clarity). (**C**) The relationship of phase travel time against the distance to the reference pixel; the phase speed of the wave in this region is estimated from a least-squares linear fit.

quiet Sun, these are rooted within the vertices and lanes defining the supergranular network. The internetwork nonmagnetic chromosphere tends to oscillate near 5 to 7 mHz in response to convective driving. In the network itself, the period shifts closer to 3 mHz (*19*). We observed (Fig. 2) that the CoMP velocity power spectrum peaks near 3.5 mHz, but relatively little of the 5-mHz power that dominates the internetwork chromosphere was evident. Perhaps the waves observed with CoMP originate from within the chromospheric network that forms the footpoints of the observed coronal loops. Recent work demonstrated that p modes with frequencies below the nominal acoustic cutoff frequency can leak into the upper chromosphere along magnetic field lines that are inclined to the gravitational field, effectively reducing the cutoff frequency (*20*–*24*). The bulk of the 5-mHz power does not penetrate the chromospheric canopy as compressive oscillation modes (*17*, *25*, *26*), and so these frequencies may not have a strong signature in the corona. The waves we observed were only those that could "tunnel" through the complex chromosphere-transition region along the magnetic field lines and then be converted near the $\beta = 1$ surface, where the plasma force balance transitions from gas dominated to magnetic field dominated to Alfvén modes. Unfortunately, the conversion mechanism is not understood or easily modeled, given the complex structure of the interface between the chromosphere and corona.

We observe a dominance of upward over downward wave propagation. Of all of the pixels with acceptable errors, only ~1% had a negative phase speed indicative of downward propagation. This suggests that the waves are converted or their energy is dissipated before they reach the opposite footpoint. Given the large curvature of the field lines over a typical wavelength, we would expect that conversion of Alfvén to MA modes would be efficient (*27*).

To evaluate the ability of these waves to heat the corona, we estimated the energy flux as

$$F_W = \rho\langle v^2\rangle c_A \quad (3)$$

where ρ is the density, v is the velocity amplitude, and c_A is the Alfvén speed. Assuming a typical value of the electron density of 10^8 cm^{-3}, we estimate $\rho \sim 2 \times 10^{-16}$ g cm^{-3}. The flux of energy propagating in the observed waves is then

$$F_W \sim 10 \text{ erg cm}^{-2} \text{ s}^{-1} \text{ (0.01 W m}^{-2}\text{)} \quad (4)$$

Because we only observed the LOS velocity, this estimate can be multiplied by a factor of 2. Even so, the flux is 4 orders of magnitude too small to balance the radiative losses even of the quiet solar corona, ~100 W m^{-2} (*28*). The amplitude of the Alfvén waves that we observed may be significantly attenuated by averaging over many unresolved waves within our spatial resolution element and along the coronal LOS. The nonthermal component of coronal emission line widths is typically ~30 km s^{-1} and temporally invariant, which, if due to unresolved Alfvén waves, could provide a steady energy flux sufficient to heat the corona.

These waves are ubiquitous in space and time. This makes them ideal candidates for "coronal seismology" (*29*, *30*), wherein the Alfvén speed (wave phase speed) can be used to measure the strength of coronal magnetic fields through the relation:

$$c_A = B/\sqrt{4\pi\rho} \quad (5)$$

where B is the magnetic field strength and ρ is the plasma density. The phase speeds obtained in this study are a projection onto the POS, that is, the speed multiplied by $\sin(i)$, where i is the angle between the LOS and the direction of wave propagation. Then, given an estimate of the density, the measured phase speeds provide an

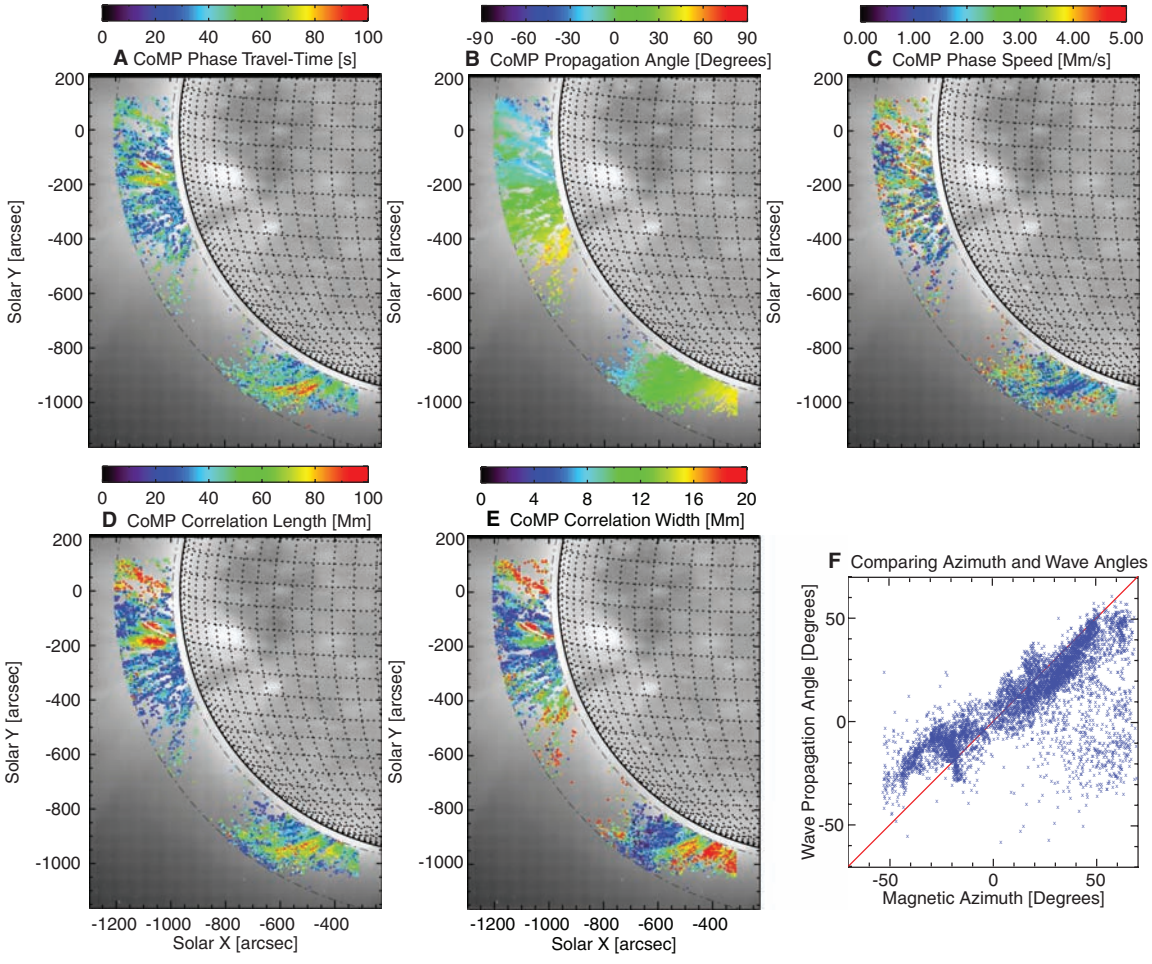

Fig. 4. The results of the CoMP travel-time analysis in the 1.05 to 1.25 R_{sun} range superimposed on the SOHO/EIT image from Fig. 1D. (**A** to **E**) The inferred wave travel time, propagation angle, phase speed, correlation length, and correlation width, respectively. Only points where the error in the phase speed from the regression analysis is less than 0.5 Mm s^{-1} and the error in the propagation angle is less than 10° are plotted. (**F**) The comparison of the inferred wave propagation angle and the measured magnetic field azimuth (Fig. 1F).

estimate of the POS component of the magnetic field. Assuming a typical electron density of 10^8 cm^{-3}, our measured phase speeds between 1.5 and 5 Mm s^{-1} correspond to projected magnetic field strengths between 8 and 26 G. We note that circular polarization measurements of coronal emission lines can provide an estimate of the LOS component of the magnetic field. Notably, seismology and polarimetry provide complementary projections of the coronal magnetic field, which can be combined to provide an estimate of both the strength and the inclination of the magnetic field. In future work, it will be possible to estimate the plasma density with CoMP observations through the intensity ratio of the FeXIII lines at 1074.7 and 1079.8 nm (*31*).

We have analyzed observations from the CoMP instrument that show an overwhelming flux of upward-propagating low-frequency waves throughout the solar corona. These waves propagate at speeds typical of Alfvén waves, and their direction of propagation mirrors the measured magnetic field direction. The waves we resolved do not have enough energy to heat the solar corona. We conclude that these ubiquitous waves are indeed Alfvénic and offer the real possibility of probing the plasma environment of the solar corona with a high degree of accuracy through coronal seismology.

References and Notes

1. H. Alfvén, *Nature* **150**, 405 (1942).
2. H. Alfvén, *Mon. Not. R. Astron. Soc.* **107**, 211 (1947).
3. D. Osterbrock, *Astrophys. J.* **134**, 347 (1961).
4. M. J. Aschwanden, L. Fletcher, C. J. Schrijver, G. Alexander, *Astrophys. J.* **520**, 880 (1999).
5. V. M. Nakariakov, L. Ofman, E. E. DeLuca, B. Roberts, J. M. Davila, *Science* **285**, 862 (1999).
6. C. E. DeForest, J. B. Gurman, *Astrophys. J.* **501**, L217 (1998).
7. I. De Moortel, J. Ireland, R. W. Walsh, *Astron. Astrophys.* **355**, L23 (2000).
8. M. A. Marsh, R. W. Walsh, *Astrophys. J.* **643**, 540 (2006).
9. M. Minarovjech *et al.*, *Sol. Phys.* **213**, 269 (2003).
10. D. R. Williams *et al.*, *Mon. Not. R. Astron. Soc.* **326**, 428 (2001).
11. J. M. Pasachoff, F. A. Babcock, K. D. Russell, D. B. Seaton, *Sol. Phys.* **207**, 241 (2002).
12. S. Koutchmy, I. D. Zhugzhda, V. Locans, *Astron. Astrophys.* **120**, 185 (1983).
13. T. Sakurai, K. Ichimoto, K. P. Raju, J. Singh, *Sol. Phys.* **209**, 265 (2002).
14. J. W. Belcher, *Astrophys. J.* **168**, 505 (1971).
15. P. Charvin, *Ann. Astrophys.* **28**, 877 (1965).
16. S. M. Jefferies *et al.*, *Astrophys. J.* **434**, 795 (1994).
17. W. Finsterle *et al.*, *Astrophys. J.* **613**, L185 (2004).
18. S. W. McIntosh, B. Fleck, T. D. Tarbell, *Astrophys. J.* **609**, L95 (2004).
19. B. W. Lites, R. Rutten, W. Kalkofen, *Astrophys. J.* **414**, 345 (1993).
20. B. De Pontieu, R. Erdélyi, I. DeMoortel, *Astrophys. J.* **624**, L61 (2005).
21. V. H. Hansteen *et al.*, *Astrophys. J.* **647**, L73 (2006).
22. S. W. McIntosh, S. M. Jefferies, *Astrophys. J.* **647**, L77 (2006).
23. S. M. Jefferies *et al.*, *Astrophys. J.* **648**, L151 (2006).
24. B. De Pontieu *et al.*, *Astrophys. J.* **655**, 624 (2007).
25. O. Wikstol, P. G. Judge, V. Hansteen, *Astrophys. J.* **501**, 895 (1998).
26. P. G. Judge, A. Pietarila, *Astrophys. J.* **606**, 1258 (2004).
27. D. Melrose, *Aust. J. Phys.* **30**, 647 (1977).
28. G. L. Withbroe, R. W. Noyes, *Annu. Rev. Astron. Astrophys.* **15**, 363 (1977).
29. E. Verwichte, C. Foullon, V. M. Nakariakov, *Astron. Astrophys.* **446**, 1139 (2006a).
30. V. M. Nakariakov, E. Verwichte, *Living Rev. Sol. Phys.* **2**, 3 (2005).
31. M. J. Penn *et al.*, *Space Sci. Rev.* **70**, 185 (1994).

32. The authors would like to thank M. Knölker and P. Weis-Taylor for comments on the manuscript. Construction of the CoMP instrument was funded by the NSF through the NCAR Strategic Initiative Fund and HAO/NCAR base funds. The effort of S.M.C. was supported by grant ATM-0541567 from NSF.

Supporting Online Material

www.sciencemag.org/cgi/content/full/317/5842/1192/DC1
Materials and Methods
Table S1
References
Movies S1 to S4

2 April 2007; accepted 27 July 2007
10.1126/science.1143304

Superconducting Interfaces Between Insulating Oxides

N. Reyren,[1] S. Thiel,[2] A. D. Caviglia,[1] L. Fitting Kourkoutis,[3] G. Hammerl,[2] C. Richter,[2] C. W. Schneider,[2] T. Kopp,[2] A.-S. Rüetschi,[1] D. Jaccard,[1] M. Gabay,[4] D. A. Muller,[3] J.-M. Triscone,[1] J. Mannhart[2]*

At interfaces between complex oxides, electronic systems with unusual electronic properties can be generated. We report on superconductivity in the electron gas formed at the interface between two insulating dielectric perovskite oxides, $LaAlO_3$ and $SrTiO_3$. The behavior of the electron gas is that of a two-dimensional superconductor, confined to a thin sheet at the interface. The superconducting transition temperature of ≅ 200 millikelvin provides a strict upper limit to the thickness of the superconducting layer of ≅ 10 nanometers.

In pioneering work, it was demonstrated that a highly mobile electron system can be induced at the interface between $LaAlO_3$ and $SrTiO_3$ (*1*). The discovery of this electron gas at the interface between two insulators has generated an impressive amount of experimental and theoretical work (*2*–*8*), in part because the complex ionic structure and particular interactions found at such an interface are expected to promote novel electronic phases that are not always stable as bulk phases (*9*–*11*). This result also generated an intense debate on the origin of the conducting layer, which could either be "extrinsic" and due to oxygen vacancies in the $SrTiO_3$ crystal or "intrinsic" and related to the polar nature of the $LaAlO_3$ structure. In the polar scenario, a potential develops as the $LaAlO_3$ layer thickness increases that may lead to an "electronic reconstruction" above some critical thickness (*5*). Another key issue concerns the ground state of such a system; at low temperatures, a charge-ordered interface with ferromagnetic spin alignment was predicted (*4*). Experimental evidence in favor of a ferromagnetic ground state was recently found (*6*). Yet, rather than ordering magnetically, the electron system may also condense into a superconducting state. It was proposed that in field effect transistor configurations, a superconducting, two-dimensional (2D) electron gas might be generated at the $SrTiO_3$ surface (*12*). It was also pointed out that the polarization of the $SrTiO_3$ layers may cause the electrons on $SrTiO_3$ surfaces to pair and form at high temperatures a superconducting condensate (*13*, *14*). In this report, we explore the ground state of the $LaAlO_3/SrTiO_3$ interface and clarify whether it orders when the temperature approaches absolute zero. Our experiments provide evidence that the investigated electron gases condense into a superconducting phase. The characteristics of the transition are consistent with those of a 2D electron system undergoing a Berezinskii-Kosterlitz-Thouless (BKT) transition (*15*–*17*). In the oxygen vacancy scenario the observation of superconductivity provides a strict upper limit to the thickness of the superconducting sheet at the $LaAlO_3/SrTiO_3$ interface.

The samples were prepared by depositing $LaAlO_3$ layers with thicknesses of 2, 8, and 15 unit cells (uc) on TiO_2-terminated (001) surfaces of $SrTiO_3$ single crystals (*5*, *18*). The films were grown by pulsed laser deposition at 770°C and 6×10^{-5} mbar O_2, then cooled to room temperature in 400 mbar of O_2, with a 1-hour oxidation step at 600°C. The fact that only heterostructures with a $LaAlO_3$ thickness greater than three uc conduct (*5*) was used to pattern the samples (*19*). Without exposing the $LaAlO_3/SrTiO_3$ interface to the environment, bridges with widths of 100 μm and lengths of 300 μm and 700 μm were structured for four-point measurements, as well as two-uc-thick $LaAlO_3$ layers for reference (*18*).

[1]Département de Physique de la Matière Condensée, University of Geneva, 24 quai Ernest-Ansermet, 1211 Genève 4, Switzerland. [2]Experimental Physics VI, Center for Electronic Correlations and Magnetism, Institute of Physics, University of Augsburg, D-86135 Augsburg, Germany. [3]School of Applied and Engineering Physics, Cornell University, Ithaca, NY 14853, USA. [4]Laboratoire de Physique des Solides, Bat 510, Université Paris-Sud 11, Centre d'Orsay, 91405 Orsay, Cedex, France.

*To whom correspondence should be addressed. E-mail: jochen.mannhart@physik.uni-augsburg.de